THE JOURNAL OF BIOLOGICAL CHEMISTRY VOL. 288, NO. 11, pp. 7580–7589, March 15, 2013

Up-regulation of Hyperpolarization-activated Cyclic Nucleotide-gated Channel 3 (HCN3) by Specific Interaction with K^+ Channel Tetramerization Domain-containing Protein 3 (KCTD3)*[S]

Received for publication, November 9, 2012, and in revised form, January 31, 2013 Published, JBC Papers in Press, February 4, 2013, DOI 10.1074/jbc.M112.434803

Xiaochun Cao-Ehlker, Xiangang Zong[1], Verena Hammelmann[1], Christian Gruner, Stefanie Fenske, Stylianos Michalakis, Christian Wahl-Schott, and Martin Biel[2]

From the Center for Integrated Protein Science CIPS-M and Zentrum für Pharmaforschung, Department Pharmazie, Ludwig-Maximilians-Universität München, 81377 Munich, Germany

Background: HCN channels are key regulators of neuronal excitability.
Results: We identify KCTD3 as a protein that specifically interacts with HCN3 in brain and up-regulates cell surface expression of this channel.
Conclusion: KCTD3 is a novel accessory subunit of neuronal HCN3 channels.
Significance: The identification of KCTD3 is an important step toward achieving a better understanding of the *in vivo* role of HCN3.

Most ion channels consist of the principal ion-permeating core subunit(s) and accessory proteins that are assembled with the channel core. The biological functions of the latter proteins are diverse and include the regulation of the biophysical properties of the ion channel, its connection to signaling pathways and the control of its cell surface expression. There is recent evidence that native hyperpolarization-activated cyclic nucleotide-gated channel complexes (HCN1–4) also contain accessory subunits, among which TRIP8b (tetratricopeptide repeat-containing Rab8b-interacting protein) has been most extensively studied. Here, we identify KCTD3, a so far uncharacterized member of the potassium channel tetramerization-domain containing (KCTD) protein family as an HCN3-interacting protein. KCTD3 is widely expressed in brain and some non-neuronal tissues and colocalizes with HCN3 in specific regions of the brain including hypothalamus. Within the HCN channel family, KCTD3 specifically binds to HCN3 and leads to a profound up-regulation of cell surface expression and current density of this channel. HCN3 can also functionally interact with TRIP8b; however, we found no evidence for channel complexes containing both TRIP8b and KCTD3. The C terminus of HCN3 is crucially required for functional interaction with KCTD3. Replacement of the cytosolic C terminus of HCN2 by the corresponding domain of HCN3 renders HCN2 sensitive to regulation by KCTD3. The C-terminal-half of KCTD3 is sufficient for binding to HCN3. However, the complete protein including the N-terminal tetramerization domain is needed for HCN3 current up-regulation. Together, our experiments indicate that KCTD3 is an accessory subunit of native HCN3 complexes.

Hyperpolarization-activated cyclic nucleotide-gated (HCN)[3] channels are broadly expressed in neurons and heart cells (1–3). The current passed by HCN channels, termed I_h (I_f or I_q), has been shown to play a key role in controlling cellular excitability. On the system level I_h is implicated with a variety of physiological functions, among which pacemaker activity in cardiac sinus node and neuronal pacemaker cell (*e.g.* in the thalamic pacemakers) has been most extensively studied (4, 5). HCN channels also contribute to several other functions including dendritic integration (6), synaptic transmission (7), modulation of motor learning (8), and hippocampal LTP (8, 9).

The four homologous HCN channel subunits (HCN1–4) are members of the voltage-gated ion channel family and, hence, most likely assemble to functional homo- or heterotetrameric channels (10–12). There is growing evidence that the pore-forming HCN channel core is associated *in vivo* with a variety of accessory proteins that regulate the biophysical properties of the channel, control cellular targeting, and/or functionally link the channel to cellular signaling pathways (13). The most extensively characterized member of the HCN channel accessory proteins is TRIP8b, which was identified in a yeast two-hybrid screen using the HCN1 C terminus as bait (14), and was later on also found in a proteomics approach for the other three HCN isoforms (15). TRIP8b is extensively spliced at the N terminus and has multiple impacts on HCN channel function. Depending on the respective N terminus TRIP8b variants can either increase or decrease cell surface expression and current density of HCN1 (16–18). Moreover, TRRI8b was found to induce a hyperpolarizing shift of the activation curve that is mediated by antagonism of the stimulatory effect of cAMP on HCN channel gating (15, 19–21). There is a variety of other proteins including filamin A (22), caveo-

* This work was support by grants from the Deutsche Forschungsgemeinschaft (DFG) and the Sonderforschungsbereich 870 (SFB 870).
[S] This article contains supplemental Fig. S1.
[1] Both authors contributed equally to this work.
[2] To whom correspondence should be addressed: Department Pharmazie, Pharmakologie für Naturwissenschaften, Ludwig-Maximilians-Universität München, Butenandtstr. 5-13, 81377 München, Germany. Tel.: +49-89218077327; Fax: +49-89218077326; E-mail: martin.biel@cup.uni-muenchen.de.

[3] The abbreviations used are: HCN, hyperpolarization-activated cyclic nucleotide-gated channel; KCTD, K^+ channel tetramerization domain.

lin-3 (23), KCR1 (24), KCNE2 (25), MINT2 (26), tamalin (26), S-SCAM (26), and several protein kinases (27–30) that have been shown to be associated with HCN channels. However, the exact physiological role of most of these proteins is less well understood than that of TRIP8b.

So far, accessory proteins have been only studied for HCN1, HCN2, and HCN4. By contrast, with the exception of the finding that the C terminus of HCN3 can principally interact with TRRIP8b in a yeast two-hybrid system (14), nothing is known about proteins regulating HCN3. HCN3 is expressed in heart and brain (31–34), but also found in peripheral nervous system (35) and kidney (36). Recent analysis of HCN3 knock-out mice has revealed that the channel is involved in shaping the ventricular action potential waveform (33). The role of HCN3 in neurons is still unknown. In general, analysis of HCN3 current has been hampered by the rather low current density obtained upon expression of this protein in heterologous systems. A possible explanation for the low expression could be the lack of accessory or regulatory subunits that are needed for proper HCN3 expression and function. To address this important issue we performed in the present study a yeast two-hybrid screen to identify proteins specifically interacting with HCN3 in mouse brain. We chose the C terminus of the HCN3 channel as bait because the corresponding domain of other HCN channels has been shown to serve as a hub for scaffolding proteins and channel regulators including TRIP8b. As a result of our study we identify and functionally characterize KCTD3, a novel member of the potassium channel tetramerization domain (KCTD)-containing protein family (37). We show that within the HCN channel family KCTD3 selectively binds to HCN3 and, thereby, increases cell surface expression and current density of this channel.

EXPERIMENTAL PROCEDURES

Yeast Two-hybrid Constructs—The cytoplasmic tail of HCN3 was amplified in PCR using pcDNA3-HCN3 (Dr. Biel, Ludwig-Maximilians-Universität München) as template and subcloned into BamHI and SalI sites of pSos vector (CytoTrap XR, Stratagene). Mouse brain cDNA library (CytoTrap XR premade library, Stratagene) was amplified and purified as described in Stratagene's instruction manual.

Mammalian Expression Vectors—Full-length KCTD3 and TRIP8bA4 cDNAs were amplified from mouse brain cDNA reversely transcribed from total RNA (Thermoscript, Invitrogen) and subcloned into pcDNA3.1B at KpnI/EcoRI sites. pcDNA3.1B contains a Myc tag sequence at the 3′-end of the multiple restriction enzyme site. KCTD3-myc and TRIP8bA4-myc were amplified using pcDNA3.1B-KCTD3 and -TRIP8bA4 as templates and subcloned into XhoI/BglI and XbaI/SpeI sites of LV-CMV-IRES-eGFP (34), respectively. For the truncated version of KCTD3, KCTD3N-myc (aa 1–87) and KCTD3C-myc (aa 88–815) were PCR amplified and subcloned into LV-CMV-IRES-eGFP via XhoI/BamHI and XhoI/BglII restriction sites, respectively. To generate mCherry-tagged TRIP8bA4, mCherry was PCR amplified and subcloned into LV-CMV-TRIP8bA4-IRES-eGFP via XhoI/SalI restriction sites to replace eGFP. Bicistronic LV-CMV-IRES-eGFP and LV-CMV-IRES-mCherry vectors were used in patch clamping and cell surface experiments to identify transfected cells via fluorescence.

The generation of the stable mammalian expression cell line of HCN3 by Flp recombinase-mediated integration (Invitrogen) was described (33). To construct pcDNA5/FRT-HCN3-HA, Infusion system (Clontech) was used to insert a hemagglutinin (HA) sequence (ISAYGITYPYDVPDYA) into the extracellular loop S3 to S4 of HCN3 (inframe between aa E193 and P194) using following primers: forward: 5′-GGA ATA ACA TAC CCA TAC GAC GTC CCA GAC TAC GCT CCA CGA CTA GAT GCT GAG GTC-3′, reverse: 5′-GTA TGG GTA TGTTAT TCC GTA TGC TGA TAT CTC CAG CTC CAC CAC TAG GAA.

To generate HCN C-terminal chimeric channels, the N terminus and transmembrane segments of HCN2 (aa 1–442) was fused to the C terminus of HCN3 (aa 353–779) to construct pcDNA3-HCN2-C3, and *vice versa* for pcDNA3-HCN3-C2 (aa 1–352 of HCN3 fused to aa 443–863 of HCN2). In detail, for the pcDNA3-HCN2-C3 construct, pcDNA3-HCN2 and pcDNA3-HCN3 were digested with HindIII/PflMI and the N terminus and transmembrane segments of HCN2 were subcloned into pcDNA3-HCN3. To generate the pcDNA3-HCN3-C2 chimera, HCN2 C terminus was isolated out of pcDNA3-HCN2 by PflMI/NotI digestion and subcloned into pcDNA3-HCN3 to replace HCN3 C terminus. For pcDNA3-HCN2-C3Δ, a fragment corresponding to aa 353–556 of HCN3 C terminus was amplified and subcloned into PflMI/NotI sits of pcDNA3-HCN2.

Tissue Culture—HEK293 cells, HCN3 stable, and HCN3-HA stable cell lines were cultured in Dulbecco's modified Eagle's medium (DMEM) supplemented with 10% fetal bovine serum (Biochrom AG), 100 units/ml penicillin and 100 units/ml streptomycin (Biochrom AG) at 37 °C and 10% CO_2. HCN3 stable and HCN3-HA stable cell lines were maintained in 100 μg/ml hygromycin B (Roth). For immunoprecipitation and biotinylation, cells were transfected using the calcium phosphate method and for immunohistochemistry and electrophysiological experiments the FuGene6 transfection reagent (Roche) was applied.

Phylogenetic Tree—For the comparison of the murine KCTD members, the protein sequence of the 21 known KCTD family members was aligned using DNAman software. An additional protein Shkbp1 was also included for being known to be closely related to KCTD3 (38). For the clarity of the figure, only the longest KCTD isoform of each family member was chosen. For the tree illustrating the phylogenetic relationship among species, the protein sequences of KCTD3 was aligned within the indicated species. The genetic distances and relatedness of the proteins have been calculated from the observed divergency. The rooted and unrooted tree was then displayed using the tree drawing software NJblot (39).

Electrophysiology—Currents were measured at room temperature from HEK293 cells stably expressing one of the four murine HCN channel types of HCN channels using the whole cell voltage-clamp technique. The coexpression of KCTD3 and TRIP8b was monitored by visualizing fluorescence (eGFP for KCTD3 and mCherry for TRIP8b). The extracellular solution was composed of (mM): 110 NaCl, 30 KCl, 1.8 $CaCl_2$, 0.5 $MgCl_2$,

5 HEPES, pH 7.4 adjusted with NaOH. The intracellular solution contained (in mM): 130 KCl, 10 NaCl, 0.5 $MgCl_2$, 1 EGTA, 5 HEPES, 3 Mg-ATP, 0.5 Na-GTP, pH 7.4 adjusted with KOH. Data were acquired at 10 kHz using an Axopatch 200B amplifier and pClamp10.2 (Molecular Devices). Voltage clamp data were analyzed off-line by using Clampfit10.2 and Origin6.1. Steady-state activation curves for HCN3 were determined by hyperpolarizing voltage steps from −140 mV to −30 mV in 10 mV increments from a holding potential of −40 mV for 3.6 s (pulse interval 20 s) followed by a step to −140 mV for 0.5 s. Currents measured immediately after the final step to −140 mV were normalized by the maximal current (I_{max}) and plotted as a function of the preceding membrane potential. Data were fitted with the Boltzmann function as described (40). The voltage protocol used for determination of current density comprised voltage steps of 1.8 s (HCN1 and HCN2, pulse interval 10 s) or 3.6 s (HCN3 and HCN4, pulse interval 20 s) from a holding potential of −40 mV to test potentials ranging from −140 mV to −40 mV in 10-mV increments. The current density was determined by dividing the current at the end of the respective test pulse (pA) by cell capacitance (pF). Activation time constants (τ_a) were determined by monoexponential function fitting the current evoked during hyperpolarizing voltage pulses to −140 mV from a holding potential of −40 mV. Deactivation time constants (τ_d) were determined at −40 mV following a prepulse of −140 mV by fit with a monoexponential function.

Detection of mRNA—*In situ* hybridization was performed as describe before (41). [α-^{35}S]UTP-labeled riboprobes corresponded to aa 650–809 of KCTD3 and 618–777 of HCN3. Specificity of the signals was verified by comparing two independent probes and by using sense probes. Northern blot was performed as described (42). ^{32}P-labeled probes corresponded to aa 52–249 of GAPDH and 650–809 of KCTD3.

Antibodies—The following primary antibodies were used: mouse monoclonal α-HCN1 (ab 84816, Abcam), rabbit polyclonal α-HCN2 (43) (Western blot) or rabbit polyclonal α-HCN2 (APC-030, Alomone) (immunofluorescence), rabbit polyclonal α-HCN3 (34) (immunofluoresence), or mouse monoclonal α-HCN3 (clone N141/28, 75–175, UC Davis/NIH NeuroMab) (immunoprecipitation and Western blot), rat monoclonal α-HCN4 (sc-58622, Santa Cruz Biotechnology), rabbit polyclonal α-KCTD3 (HPA015142, Sigma) (immunoprecipitation and Western blot), or goat polyclonal α-KCTD3 (N-15, sc-164721, Santa Cruz Biotechnology) (immunofluoresence), mouse monoclonal α-TRIP8b (clone N212/7, 75–243, UC Davis/NIH NeuroMab), mouse monoclonal α-Myc (9B11, Cell Signaling/New England BioLabs Inc), mouse monoclonal α-HA-tag (HA.11 clone 16B12, MMS-101P, Covance), mouse monoclonal α-MAP2 (mAb HM2, Sigma), and mouse monoclonal α-Na, K-ATPase α subunit (clone α5, developed by D.M. Fambrough, obtained from the Developmental Studies Hybridoma Bank). The HRP-conjugated secondary antibodies used in Western blot were obtained from GE Healthcare (UK Limited). All fluorescent secondary antibodies were purchased from Jackson ImmunoResearch.

Immunoprecipitation—Transfected HEK293 cells were lysed for *in vitro* immunoprecipitation (50 mM Tris-HCl pH 7.4, 150 mM NaCl, 1 mM EDTA, 1% Triton X-100) containing proteinase inhibitors (PI) (complete, EDTA-free proteinase inhibitor mixture tablets, Roche). For *in vivo* immunoprecipitation, mouse brains were homogenized in lysis buffer (see above) and immunoprecipitation procedure was performed as described (10).

Immunofluorescent Staining—The procedure of staining cells and sagital brain slices was described previously (27). All slices were visualized using an epifluorescence microscope (Axioskop 2 with HMRc-Kamera, Zeiss) and a laser-scanning confocal microscope (LSM510 Meta, Zeiss).

Surface Biotinylation—Cell surface proteins were labeled with 0.8 mM non-cell-permeable sulfo-NHS-SS-biotin (Pierce) and precipitated using streptavidin-agarose beads (Pierce) as described (44). Quantitative Western blots were performed on both total and biotinylated surface proteins using NIH ImageJ software. The percentages of surface HCN3 in total proteins were calculated and normalized to the expression of the Na,K-ATPase α subunit.

RESULTS

Identification of KCTD3 in a Yeast Two-hybrid Screen with Mouse Brain cDNA—To identify proteins that specifically interact with HCN3 we analyzed a mouse brain cDNA library in a yeast two-hybrid screen (Y2H; Cyto Trap, Stratagene) using the complete C terminus of murine HCN3 (aa 353–779) as a bait (Fig. 1*A*). Clones positive for interaction with the bait were isolated, sequenced, and tested for interaction with HCN3 using GST pull down assays (data not shown). Among the 35 clones that emerged from the screen two clones (c#487 and c#35) represented partial cDNAs of a so-far uncharacterized protein, termed KCTD3 that was originally isolated as renal tumor antigen (NY-REN-45) (45) (Fig. 1*B*). KCTD3 belongs to the large family of KCTD (potassium (K^+) channel tetramerization domain-containing) proteins that in mouse genome comprises 22 members (Fig. 1*C*). As a structural hallmark all KCTD family members, including KCTD3, contain a bric-à-brac, tramtrak, and broad complex (BTB) motif at their N terminus, which is homologous to the tetramerization (T1) domain of voltage gated K^+ channels (37, 46). The sequences downstream of the BTB motif are not conserved within the KCTD family and display large sequence diversity. KCTD3 shares about 55% sequence identity to its closest relative, the SETA-binding protein 1 (SB1, synonymous name: SH3KBP1-binding protein 1) that was identified in tumorigenic astrocytes (supplemental Fig. S1) (38). KCTD3 and SB1 contain five WD repeats (47, 48) downstream of their BTB domain that are not present in other KCTD proteins (supplemental Fig. S1). The cDNA of KCTD3 comprises 3.7 kb, which is consistent with the size of the mRNA detected in Northern blot (Fig. 1*D*). Transcripts of KCTD3 were detected in several tissues including brain, liver, kidney, and heart. Using an antibody directed against KCTD3, a 90 kDa protein was detected in mouse brain (Fig. 1*E*), which corresponds well to the theoretical protein size of 89.9 kDa (815 aa) as predicted from the cDNA.

Expression of KCTD3 in Mouse Brain and Specific Interaction with HCN3—Next, we examined the interaction between KCTD3 and HCN3 in mouse brain. Using an antibody specific

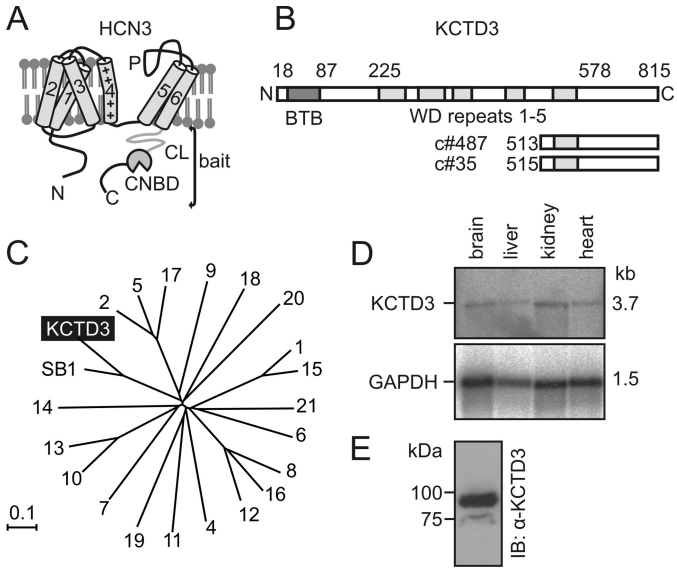

FIGURE 1. **Identification of KCTD3 as HCN3-interacting protein in mouse brain.** *A*, domain structure of HCN3. 1–6, transmembrane helices 1–6 including positively charged ("+") fourth helix; *P*, pore loop; *CL*, C-linker, *CNBD*, cyclic nucleotide-binding domain. The complete cytosolic C terminus was used as bait in a yeast two-hybrid (Y2H) screen. *B*, schematic representation of the KCTD3 protein. Numbers on top of the scheme mark the borders of the BTB domain (BTB, *red*), and the five WD (*green*) repeats. The two partial KCTD3 clones (c#487 and c#35) identified in the 2YH screen are shown below the full-length KCTD3. *C*, phylogenetic tree of the KCTD superfamily comprising 22 members in the mouse genome. The proteins are designated with numbers (*e.g.* "4" means KCTD4) or, in case of KCTD3 and its closest relative SB1, with the complete names. The tree was created using NJ BLOT. The branch distance was determined by observed divergency. The scale bar indicates the degree of genetic divergence in arbitrary units. *D*, Northern blot analysis of KCTD3 revealing mRNA expression in mouse tissues. The size of the KCTD3 transcript (3.7 kb) is indicated. *Lower panel*, as loading control the blot was reprobed for GAPDH mRNA expression. *E*, Western blot analysis of KCTD3 in mouse brain lysate using rabbit polyclonal anti-KCTD3 antibody.

for HCN3, a 90 kDa protein corresponding to KCTD3 was immunoprecipitated from total brain lysates of wild type but not of HCN3 knock-out mice (Fig. 2*A*). Similarly, HCN3 was detected in immunoprecipitated materials obtained with an anti-KCTD3 antibody (Fig. 2*A*). HCN3 was also precipitated with an antibody specific for TRIP8b, which is consistent with findings of Santoro *et al.* (14). Importantly, however, TRIP8b was not immunoprecipitated with an anti-KCTD3 antibody in wild type mice, and *vice versa* (Fig. 2*A*). These results implicated that KCTD3 and TRIP8b are not part of the same HCN3 complexes. Unlike TRIP8b, which interacts with all four HCN channel types (14), KCTD3 is highly specific for HCN3. While anti-KCTD3 antibody immunoprecipitated HCN3 channel, there was no detectable interaction with HCN1, HCN2, or HCN4 in mouse brain (Fig. 2*B*).

In situ hybridization revealed that transcripts of HCN3 and KCTD3 were both present in mouse brain although the expression level of KCTD3 was generally higher than that of HCN3 (Fig. 3*A*). Using immunohistochemistry we identified large degree overlapping of protein expression in some brain regions including the hypothalamus (Fig. 3, *C* and *D*), laterodorsal tegment and raphe (median and dorsal) in the midbrain (data not shown). As shown in the confocal images (Fig. 3*D*), compared with HCN3, KCTD3 was more ubiquitously distributed within the cells, and the co-localization was mainly observed on the cell surface. Costaining with an antibody specific for the neuronal marker MAP2 (microtubule-associated protein 2) (49) confirmed that both HCN3 and KCTD3 are expressed in neurons (Fig. 3, *C--F*, *panels* at the *right hand side*). Overall, overlap in HCN3 and KCTD3 expression was only partial since there were regions that displayed high HCN3 but medium level KCTD3 expression, such as olfactory bulb (Fig. 3*G*) while other parts of the brain such as cerebellum (molecular layers and white matter) displayed low HCN3 but strong KCTD3 expression (Fig. 3*H*). In most regions expressing HCN3, other HCN channel types were also present (Fig. 3*I* showed expression of HCN1, HCN2, and HCN4 in hypothalamus). These findings suggested that 1) KCTD3 is assembled with HCN3 in a subset of HCN3 complexes and 2) that KCTD3 also fulfills functions in brain that are not associated with HCN3.

KCTD3 Increases Current Density and Cell Surface Expression of HCN3—To study functional effects of KCTD3 we examined HCN3-mediated currents from a HEK293 cell line stably expressing HCN3 (Fig. 4). Untransfected HEK293 cells expressed none or very low level of endogenous KCTD3 (data not shown), which allowed us to examine the effects of exogenous KCTD3 on HCN3 current. HCN3 currents were rather small in the absence of KCTD3 (-64.4 ± 7.25 pA/pF at -140 mV, $n = 20$) (Fig. 4, *A* and *C*). Coexpression of KCTD3 profoundly up-regulated the current leading to an about 3–4-fold increase of current density (-262 ± 30.7 pA/pF at -140 mV, $n = 21$) (Fig. 4, *B* and *C*). By contrast KCTD3 neither affected voltage-dependence of activation (Fig. 4*D*) nor did it have an impact on the activation and deactivation kinetics of HCN3 currents (τ_a: HCN3: 572 ± 21.2 ms, $n = 20$, and HCN3+KCTD3: 531 ± 23.8 ms, $n = 21$, $p = 0.21$; τ_d: HCN3: 1.74 ± 0.10 s, $n = 12$, and HCN3+KCTD3, 1.52 ± 0.11 s, $n = 10$, $p = 0.16$). Importantly, the stimulatory effect of KCTD3 was specific for HCN3 and was not observed in stable HCN1, HCN2 or HCN4 cell lines cotransfected with KCTD3 (Fig. 4*E*). TRIP8b (splice variant A4; Ref. 16) increased HCN3 currents to the same extent as KCTD3 (-327 ± 29.1 pA/pF at −140 mV, $n =$ 21). However, current density observed upon coexpression of both TRIP8b and KCTD3 (-285 ± 27.0 pA/pF at −140 mV, $n =$ 22) did not differ from current density observed with either KCTD3 or TRIP8b alone (Fig. 4*F*). Finally, TRIP8b alone, or co-expressed with KCTD3 did not significantly alter the voltage-activation of HCN3 ($V_{0.5}$: HCN3: -100 ± 0.77 mV, $n = 20$, HCN3+TRIP8bA4: -101 ± 1.12 mV, $n = 21$, HCN3+TRIP8bA4+KCTD3: -99.1 ± 1.02 mV, $n = 22$, $p =$ 0.31).

To examine the mechanism by which KCTD3 increased HCN3 current density we performed cell surface biotinylation in combination with immunoprecipitation in the HEK293 cell line stably expressing HCN3. Fig. 5*A* shows that the amount of biotinylated HCN3 (*i.e.* channel protein that was accessible from the extracellular side) was significantly increased upon coexpression of KCTD3 (~2-fold, Fig. 5*A*, *right panel*). The difference between the increase in current density (3–4-fold) and protein surface level (~2-fold) was most likely due to the fact that in electrophysiology only the green fluorescent cells (as a marker for KCTD3) are analyzed while the biochemical assay also includes cells that were not successfully transfected with

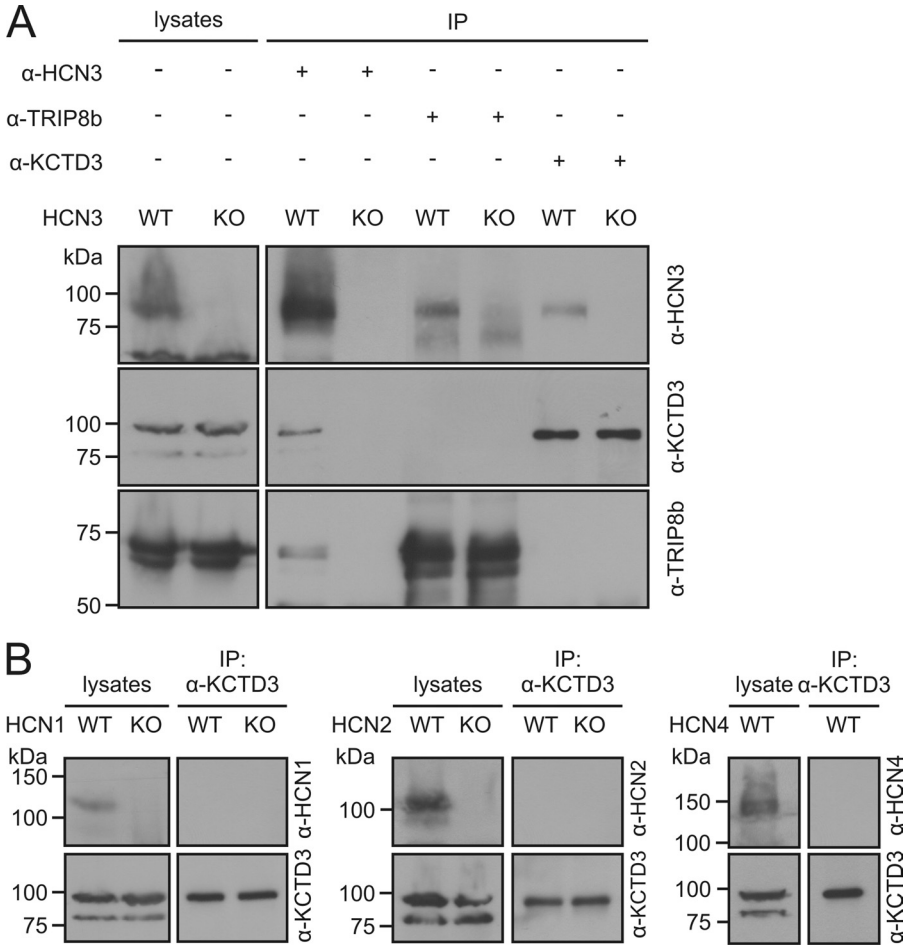

FIGURE 2. **Specific interaction between KCTD3 and HCN3 channels in mouse brain.** *A*, identification of distinct HCN3-KCTD3 and HCN3-TRIP8b complexes. Protein lysates from brain tissue of wild type (*WT*) and HCN3 knock-out (*KO*) mice were immunoprecipitated with anti-HCN3, anti-KCTD3 or anti-TRIP8b antibodies. The precipitated samples were analyzed in Western blots using antibodies against HCN3, KCTD3, or TRPIP8b as indicated. *B*, KCTD3 does not bind to HCN1, HCN2, or HCN4. Brain lysates were immunoprecipitated with anti-KCTD3 antibody and immunoblotted with HCN channel-specific antibodies. For HCN1 and HCN2, analysis was performed in WT and KO mice, for HCN4 analysis was only performed in WT mice because HCN4 KO mice die *in utero*.

KCTD3. We further explored the hypothesis that KCTD3 increases cell surface expression of HCN3 by generating a stable cell line expressing a HCN3 mutant containing a modified HA tag in the extracellular S3-S4 loop. Staining of the permeabilized cell line with anti-HCN3 or anti-HA antibodies revealed no principal difference in expression levels of wild type or HA-tagged HCN3 (Fig. 5*B*). As found for other HCN channels overexpressed in heterologous systems most of the HCN3 immunostaining was localized intracellularly. In non-permeabilized cells the immunostaining obtained with an anti-HA antibody was just at the detection level indicating that very low amounts of HCN3 were in the plasma membrane (Fig. 5*C*). However, when a KCTD3-IRES-eGFP vector was transfected into the HCN3-HA cell line a robust HCN3 signal was detected on the membrane (Fig. 5*D*). In combination, these finding strongly suggested that KCTD3 increased cell surface expression of HCN3 and, hence, HCN3-mediated current amplitudes.

Molecular Determinants of the Functional Interaction between KCTD3 and HCN3—In the Y2H screen KCTD3 was identified to bind to the HCN3 C terminus. We were thus wondering whether the stimulatory effect of KCTD3 could be transferred to other HCN channels by transplanting the HCN3 C terminus. Indeed, unlike wild type HCN2, a chimeric channel composed of the N terminus and transmembrane core of HCN2 fused with the complete cytosolic C terminus of HCN3-bound KCTD3 (Fig. 6*A*) and was profoundly up-regulated by KCTD3 (Fig. 6*D*; HCN2-C3: -161 ± 32.1 pA/pF at -140 mV, ($n = 29$); HCN2-C3+KCTD3: -558 ± 75.9 pA/pF at -140 mV, ($n = 20$)). Binding of KCTD3 did not require the complete HCN3 C terminus since it was also observed in a HCN2-HCN3 chimera lacking the sequence downstream of the CNBD (HCN2-C3Δ) (Fig. 6*B*). In contrast, HCN3 lost its capability to bind KCTD3 and was no longer up-regulated by this protein when its C terminus was replaced by the corresponding domain of HCN2 (Fig. 6, *C* and *D*). We finally asked which protein domains in KCTD3 are crucial for its effect on HCN3. The N-terminal fragment that contains the first 87 residues including the BTB motif of KCTD3 (KCTD3N) did not bind to HCN3 (Fig. 6*E*). In contrast, a truncated KCTD3 lacking the N-terminal BTB (KCTD3C) readily bound to HCN3 (Fig. 6*E*). However, neither KCTD3N nor KCTD3C when expressed alone increased HCN3 currents. However, when both fragments were coexpressed in the HCN3 stable cell line current density was increased about 3-fold with respect to HCN3 alone (Fig. 6*F*). This finding indicated that the N terminus of KCTD3

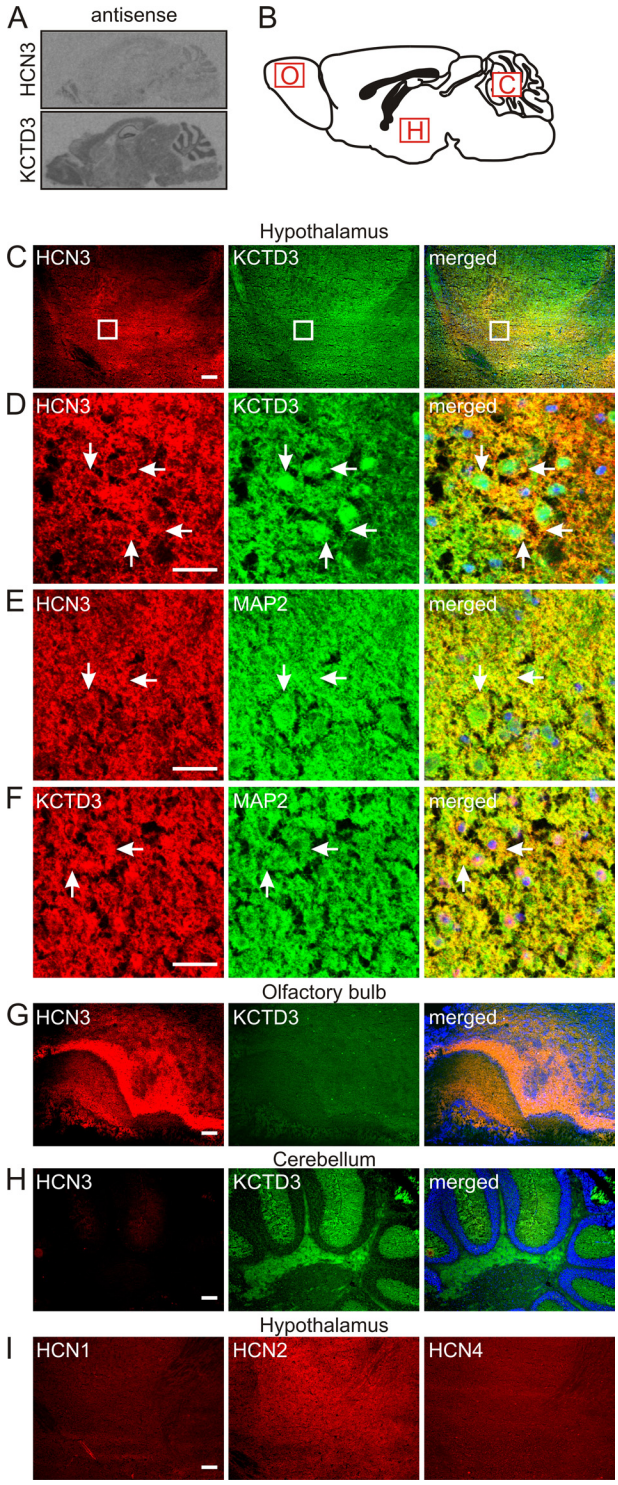

FIGURE 3. **Colocalization of KCTD3 and HCN3 in mouse brain.** *A*, sagittal sections of mouse brain hybridized with antisense RNA probes for HCN3 (*upper panel*) and KCTD3 (*lower panel*). *B-I*, immunohistochemical analysis of KCTD3 expression in mouse brain. Images from *C*, *G*, *H*, and *I* are obtained by epifluorescence microscopy and images in *D*, *E*, and *F* are analyzed with confocal microscopy. *B*, scheme of mouse brain (sagittal section). Regions selected for analysis are marked by *red boxes*. *O*, olfactory bulb; *H*, hypothalamus; *C*, cerebellum. *C*, costaining of hypothalamus with anti-HCN3 (*red*) and anti-KCTD3 (*green*) antibodies. The panel at the *right* shows the merged images. *D*, area demarcated by the white boxes in *row C* at higher magnification with confocal microscope. *E*, colabeling of hypothalamus with antibodies against HCN3 and the neuronal marker MAP2. *F*, colabeling of hypothalamus with antibodies against KCTD3 and the neuronal marker MAP2. *G* and *H*, costaining of olfactory bulb (*G*) and cerebellum (*H*) with anti-HCN3 and anti-KCTD3 antibodies. The *right panels* show the merged images, respectively. Nuclei were visualized with Hoechst dye (*blue*). *I*, staining of hypothalamus with anti-HCN1, anti-HCN2, and anti-HCN4 antibodies. *Scale bars:* 200 μm (*C*, *G*, *H*, and *I*), and 25 μm (*D*, *E*, and *F*).

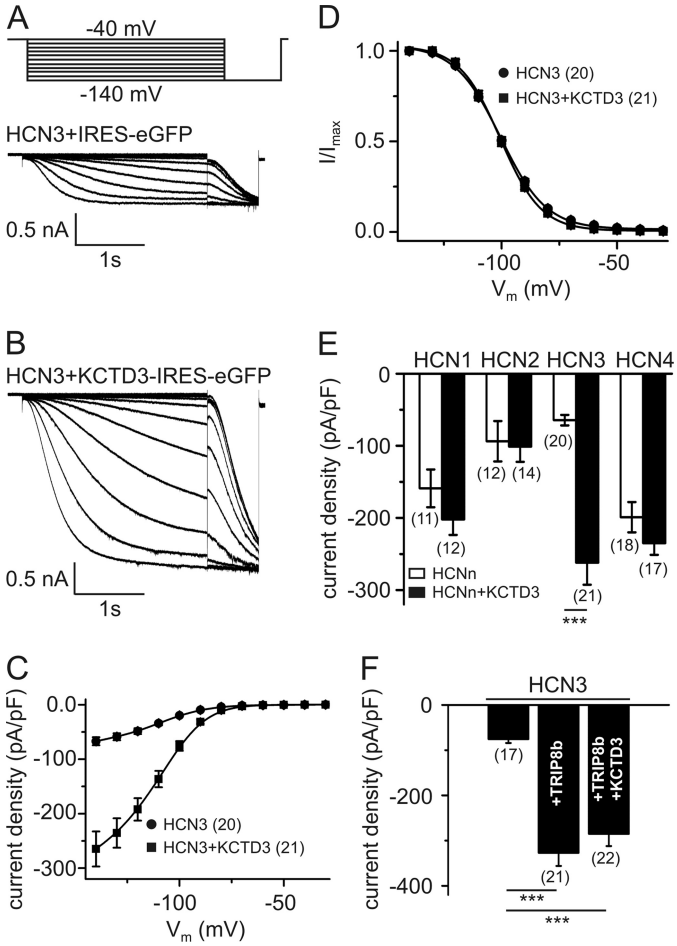

FIGURE 4. **Up-regulation of HCN3 current density by KCTD3.** *A* and *B*, representative family of HCN3 current traces obtained from a stable HCN3 cell line (HEK293) transfected with either IRES-eGFP (*A*) or KCTD3-IRES-eGFP (*B*). Currents were evoked by stepping for 3.6 s from a holding potential of −40 mV to membrane potentials ranging from −140 to −40 mV in 10 mV increments as indicated in the pulse protocol in *panel A*. *C*, current-voltage relationship of HCN3 current in the absence (*circles*) and presence (*squares*) of KCTD3. *D*, activation curves of HCN3 (*circles*) and HCN3+KCTD3 (*squares*). *E*, current densities at −140 mV of HCN1–4 in the absence (*open bars*) and presence (*closed bars*) of KCTD3. *F*, current density of HCN3 at −140 mV as compared with HCN3 coexpressed with TRIP8b alone or TRIP8b plus KCTD3. The number of cells tested is given in parentheses in *C-F*. ***, $p < 0.001$. Values are given as mean ± S.E.

although not directly binding to the HCN3 channel is required to confer the stimulatory effect of KCTD3.

DISCUSSION

In this study we report the specific interaction between HCN3 and KCTD3, a so-far uncharacterized member of the KCTD protein family, in mouse brain. KCTD3 is a soluble protein containing a number of domains that can confer protein-protein interactions. As a hallmark of the KCTD family the N terminus of KCTD3 harbors a BTB motif. BTB motifs are found in numerous proteins with diverse functions including transcription repression (50), cytoskeleton regulation (51), and protein ubiquitination/degradation (52, 53). BTB motifs can

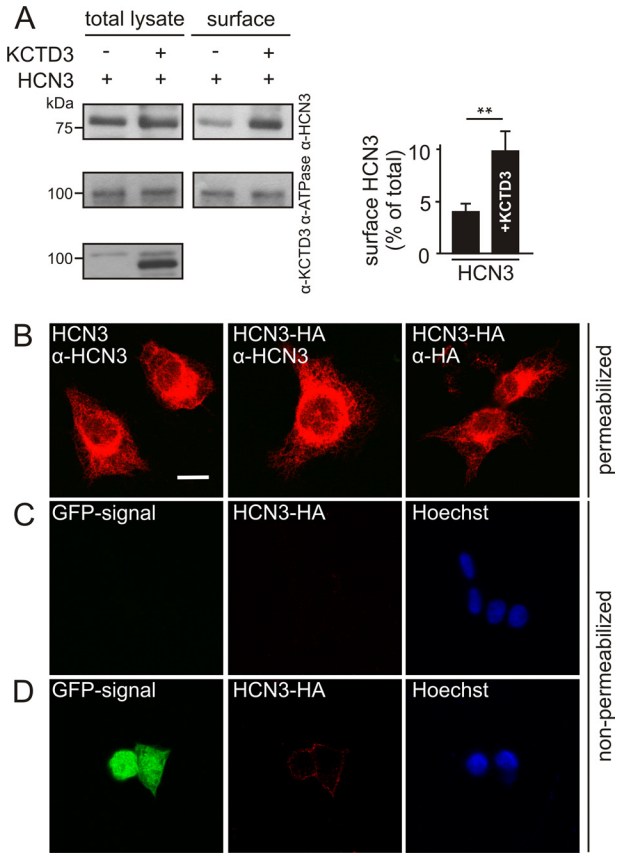

FIGURE 5. **KCTD3 enhances cell surface expression of HCN3.** *A*, cell surface biotinylation of a stable HCN3-HEK293 cell line tranfected with KCTD3 or empty vector. Biotinylated cells were precipitated using strepavidin-agarose beads and along with total lysates analyzed by Western blotting using antibodies recognizing HCN3 (*upper panel*), Na, K-ATPase α subunit (*middle panel*), or KCTD3 (*lower panel*, only total lysates). *Right panel*, quantification of Western blot results from four independent experiments. The percentage of surface HCN3 in total proteins was normalized with that of Na,K-ATPase α subunit. **, $p < 0.01$. Values are given as mean ± S.E. *B-D*, images were taken with confocal microscopy. *B*, subcellular localization of wild-type and an HA-tagged HCN3 (HCN3-HA). HEK293 cell lines stably expressing HCN3 or HCN3-HA, were fixed, permeabilized, and immunostained with either anti-HCN3 or anti-HA antibodies. *C* and *D*, HCN3-HA surface expression in the absence and presence of KCTD3. HCN3-HA-expressing HEK293 cells, either non-transfected (*C*) or transfected with KCTD3-IRES-eGFP (*D*) were stained with anti-HA antibody, followed by Cy3 anti-mouse IgG at 4 °C without prior permeabilization. Under these conditions the antibody detects only proteins facing the extracellular compartment (*middle panels* in *rows C* and *D*). Following the staining of extracellular HA epitope, cells were then fixed, permeabilized, and stained with Hoechst Dye (*blue*) to visualize the cell bodies (*right panels* in *rows C* and *D*). Note, the KCTD3-IRES-eGFP vector produces GFP and KCTD3 proteins separately, therefore, the GFP signal within the cells indicates the transfected cells instead of the cellular localization of KCTD3. *Scale bar B-D*: 10 μm.

interact with non-BTB proteins but can also self-associate. The BTB domain of KCTD family members reveals structural similarity (25%) to the T1-domain of some voltage-gated K^+ channels (for example, Kv2.1) that confers tetramerization of these channels and serves as a platform for binding of the K^+ channel β subunits. KCTD3 also contains five homologous WD repeat domains. WD repeats comprise 40–60 residue sequences that fold into a β propeller structure (47, 48). Like the BTB domain WD repeats are found in numerous proteins where they form a docking platform on which protein complexes assemble. Interestingly, KCTD8, 12a/b, and 16 have been recently identified as accessory subunits of $GABA_B$ receptors. There is evidence that the native $GABA_B$ receptor is a 1:1 complex of the $GABA_{B1/B2}$ dimer and a KCTD tetramer (54), whereas also KCTD pentamers were reported (55). In analogy with this stoichiometry, a KCTD3 multimer could be also part of the native HCN3 complex. In this context it is important to note that the BTB domain is not required for binding to KCTD3. Our Y2H and immunoprecipitation experiments rather indicate that sequences downstream of WD4 confer binding to HCN3 leaving the BTB free for other interactions including homotetramerization or interaction with other cellular proteins.

Our results show that KCTD3 profoundly up-regulates HCN3 current density (about 3–4-fold) while it does not affect the principal biophysical properties of the HCN3 channel including its voltage dependence and kinetics. Cell surface labeling experiments indicate that current up-regulation induced by KCTD3 goes along with a strong increase of cell surface expression suggesting that KCTD3 is needed for proper trafficking of HCN3 complexes to the membrane. Notably, the other HCN channel types neither bind KCTD3 nor are they functionally regulated by this protein. However, at least in HCN2, both properties can be transferred by transplanting the HCN3 C terminus. Thus, it can be assumed that the structural determinants conferring KCTD3-specific effects reside in the HCN3 C terminus. Surprisingly, the deletion of the sequence downstream of the CNBD (distal C terminus), which is most diverse between HCN3 and the other three HCN channel types did not abolish KCTD3 binding. An explanation for this result is that the amino acid differences in the C-linker-CNBD sequence (23 exchanges out of 172 residues) underlie the different responsiveness to KCTD3. With regard to KCTD3 we found that the C-terminal third of the protein (starting from residue 513) is fully sufficient to interact with HCN3. Interestingly, however, the complete protein is needed for functional regulation of HCN3. Moreover, the BTB domain and the rest of KCTD3 can assemble autonomously with the HCN3 channel since they up-regulate the channel when coexpressed as distinct soluble proteins.

We also explored the relationship of KCTD3-dependent and TRIP8b-dependent regulation of HCN3. In agreement with a previous report (14) we found that HCN3 binds to TRIP8b in HEK293 cells and in native brain tissue. Moreover, the major hippocampal TRIP8b isoform enhancing HCN1 (TRIP8bA4) (16, 17) also profoundly increased HCN3 current density. Importantly, however, coexpression of HCN3 together with both KCTD3 and TRIP8bA4 did not exert additive effects on the current amplitudes. This finding might be explained by the fact that KCTD3 and TRIP8 cannot bind to the same HCN3 channel complex. Indeed, in coimmunoprecipitation experiments in mouse brain we found no evidence for complexes containing both TRIP8b and KCTD3. By contrast, we could clearly detect distinct HCN3-KCTD3 and HCN3-TRIP8b protein complexes in mouse brain. Taken together, these results indicate that mouse brain contains at least two principal types of HCN3 complexes, one of which is associated with KCTD3 while the other includes TRIP8b. It is conceivable that the coexistance of different HCN3 channel complexes along with the presence of other HCN channel isoforms that together underlie

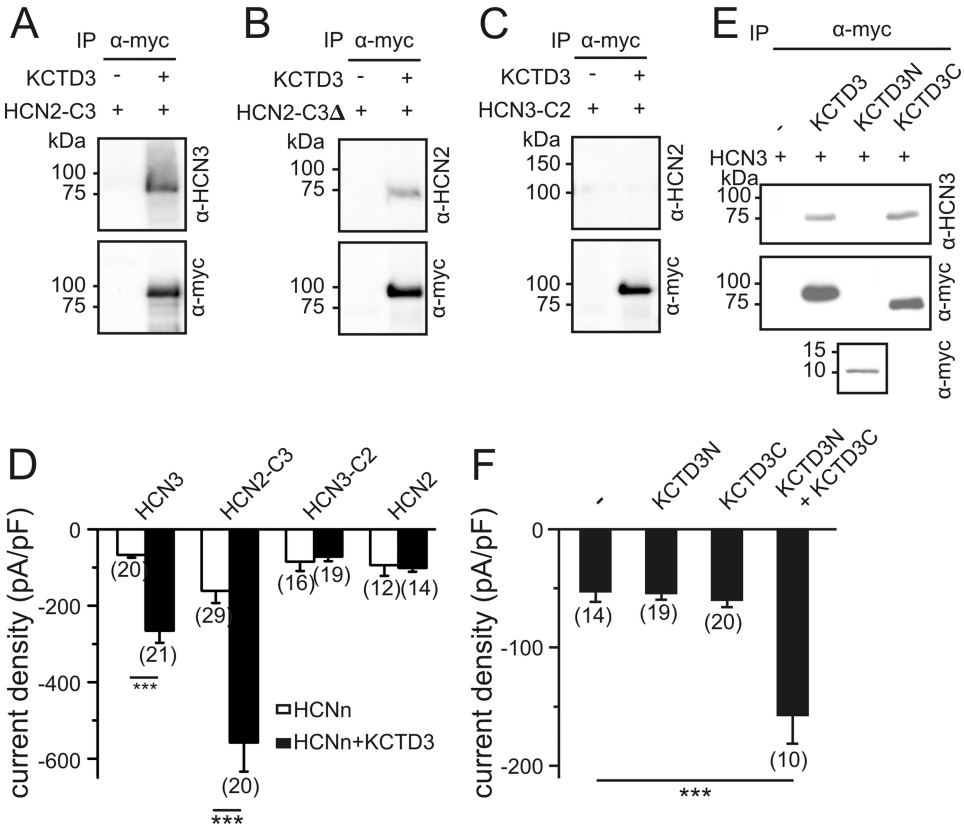

FIGURE 6. **Identification of functional domains conferring the stimulatory effect of KCTD3.** HCN channel chimeras containing the HCN2 channel core (cytosolic N terminus and transmembrane region) fused to the HCN3 cytosolic C terminus (HCN2-C3) (*A*) or to the HCN3 cytosolic C terminus lacking the sequence downstream of CNBD (HCN2-C3Δ) (*B*) or the HCN3 core fused to the HCN2 C terminus (HCN3-C2) (*C*) were expressed in HEK293 cells in the absence or presence of Myc-tagged KCTD3. Cells were immunoprecipitated with anti-Myc antibody and analyzed in Western blotting with anti-HCN3 (*A*), anti-HCN2 (*B* and *C*) and anti-Myc antibodies (*A-C*) as indicated. *D*, current densities at −140 mV of HCN channel constructs in the absence (*open bars*) and presence (*closed bars*) of KCTD3. *E*, HEK293 cells stably expressing HCN3 were transfected with KCTD3-myc, KCTD3N-myc (aa 1–87 containing the BTB-domain), or KCTD3C-myc (aa 88–815). Cell lysates were immunoprecipitated using anti-Myc antibodies and analyzed in Western blotting with anti-Myc and anti-HCN3 antibodies. *F*, current densities of HCN3-mediated currents at −140 mV in the absence and presence of different KCTD3 constructs. ***, $p < 0.001$. Values are given as mean ± S.E.

the netto I_h in a neuron strongly complicates the analysis of KCTD3-mediated effects *in vivo*.

In agreement with the coimmunoprecipitation data immunostainings revealed colocalization of KCTD3 and HCN3 in several brain region including hypothalamic neurons and several regions in the midbrain (median and dorsal raphe and laterodorsal tegment). In most regions of the brain (*e.g.* in cerebellum) KCTD3 levels were significantly higher than those of HCN3. However, there were also regions displaying profound HCN3 but medium level KCTD3 expression (*e.g.* olfactory bulb). Thus, HCN3 may be assembled with either KCTD3 or other accessory subunits such as TRIP8b depending on the type of neuron.

KCTD3 is also expressed in several non-neuronal tissues. In two of these tissues, heart muscle (33) and kidney (45), HCN3 was also detected suggesting that KCTD3-HCN3 complexes may exist outside of the brain. It is also likely, that both in brain and in non-neuronal tissues KCTD3 function may extend beyond the regulation of HCN3. In support of such a promiscuity, the KCTD proteins of the $GABA_B$ receptor complex were also detected in cell types containing no $GABA_B$ receptors (56).

In cardiomyoctes, HCN3 was recently shown to confer a depolarizing background current that regulates the resting membrane potential and contributes to the shape of the action potential (33). Whether HCN3 fulfills similar functions in neurons is currently unclear. However, it is tempting to speculate that enhanced cell surface targeting and, as a result, increased current density may play a crucial role in the physiological role of this channel.

In conclusion, our study identified for the first time an accessory subunit that is specifically associated with the HCN3 channel. This finding is an important step toward achieving a deeper understanding of the regulation and function of this as yet only poorly characterized channel.

Acknowledgments—We thank UC Davis/NIH NeuroMab Facility for developing and providing the monoclonal antibodies α-HCN3 (clone N141/28, 75-175) and α-TRIP8b (clone N212/7, 75-243).

REFERENCES

1. Biel, M., Wahl-Schott, C., Michalakis, S., and Zong, X. (2009) Hyperpolarization-activated cation channels: from genes to function. *Physiol. Rev.* **89,** 847–885
2. Craven, K. B., and Zagotta, W. N. (2006) CNG and HCN channels: two peas, one pod. *Annu Rev. Physiol.* **68,** 375–401
3. Frère, S. G., Kuisle, M., and Lüthi, A. (2004) Regulation of recombinant and native hyperpolarization-activated cation channels. *Mol. Neurobiol.* **30,** 279–305

4. Baruscotti, M., Barbuti, A., and Bucchi, A. (2010) The cardiac pacemaker current. *J. Mol. Cell Cardiol.* **48,** 55–64
5. Robinson, R. B., and Siegelbaum, S. A. (2003) Hyperpolarization-activated cation currents: from molecules to physiological function. *Annu. Rev. Physiol.* **65,** 453–480
6. Magee, J. C. (1999) Dendritic lh normalizes temporal summation in hippocampal CA1 neurons. *Nat. Neurosci.* **2,** 508–514
7. Huang, Z., Lujan, R., Kadurin, I., Uebele, V. N., Renger, J. J., Dolphin, A. C., and Shah, M. M. (2011) Presynaptic HCN1 channels regulate Cav3.2 activity and neurotransmission at select cortical synapses. *Nat. Neurosci.* **14,** 478–486
8. Nolan, M. F., Malleret, G., Lee, K. H., Gibbs, E., Dudman, J. T., Santoro, B., Yin, D., Thompson, R. F., Siegelbaum, S. A., Kandel, E. R., and Morozov, A. (2003) The hyperpolarization-activated HCN1 channel is important for motor learning and neuronal integration by cerebellar Purkinje cells. *Cell* **115,** 551–564
9. Tsay, D., Dudman, J. T., and Siegelbaum, S. A. (2007) HCN1 channels constrain synaptically evoked Ca^{2+} spikes in distal dendrites of CA1 pyramidal neurons. *Neuron* **56,** 1076–1089
10. Much, B., Wahl-Schott, C., Zong, X., Schneider, A., Baumann, L., Moosmang, S., Ludwig, A., and Biel, M. (2003) Role of subunit heteromerization and N-linked glycosylation in the formation of functional hyperpolarization-activated cyclic nucleotide-gated channels. *J. Biol. Chem.* **278,** 43781–43786
11. Whitaker, G. M., Angoli, D., Nazzari, H., Shigemoto, R., and Accili, E. A. (2007) HCN2 and HCN4 isoforms self-assemble and co-assemble with equal preference to form functional pacemaker channels. *J. Biol. Chem.* **282,** 22900–22909
12. Brewster, A. L., Bernard, J. A., Gall, C. M., and Baram, T. Z. (2005) Formation of heteromeric hyperpolarization-activated cyclic nucleotide-gated (HCN) channels in the hippocampus is regulated by developmental seizures. *Neurobiol. Dis.* **19,** 200–207
13. Lewis, A. S., Estep, C. M., and Chetkovich, D. M. (2010) The fast and slow ups and downs of HCN channel regulation. *Channels (Austin)* **4,** 215–231
14. Santoro, B., Wainger, B. J., and Siegelbaum, S. A. (2004) Regulation of HCN channel surface expression by a novel C-terminal protein-protein interaction. *J. Neurosci.* **24,** 10750–10762
15. Zolles, G., Wenzel, D., Bildl, W., Schulte, U., Hofmann, A., Müller, C. S., Thumfart, J. O., Vlachos, A., Deller, T., Pfeifer, A., Fleischmann, B. K., Roeper, J., Fakler, B., and Klöcker, N. (2009) Association with the auxiliary subunit PEX5R/Trip8b controls responsiveness of HCN channels to cAMP and adrenergic stimulation. *Neuron* **62,** 814–825
16. Lewis, A. S., Schwartz, E., Chan, C. S., Noam, Y., Shin, M., Wadman, W. J., Surmeier, D. J., Baram, T. Z., Macdonald, R. L., and Chetkovich, D. M. (2009) Alternatively spliced isoforms of TRIP8b differentially control h channel trafficking and function. *J. Neurosci.* **29,** 6250–6265
17. Santoro, B., Piskorowski, R. A., Pian, P., Hu, L., Liu, H., and Siegelbaum, S. A. (2009) TRIP8b splice variants form a family of auxiliary subunits that regulate gating and trafficking of HCN channels in the brain. *Neuron* **62,** 802–813
18. Piskorowski, R., Santoro, B., and Siegelbaum, S. A. (2011) TRIP8b splice forms act in concert to regulate the localization and expression of HCN1 channels in CA1 pyramidal neurons. *Neuron* **70,** 495–509
19. Santoro, B., Hu, L., Liu, H., Saponaro, A., Pian, P., Piskorowski, R. A., Moroni, A., and Siegelbaum, S. A. (2011) TRIP8b regulates HCN1 channel trafficking and gating through two distinct C-terminal interaction sites. *J. Neurosci.* **31,** 4074–4086
20. Han, Y., Noam, Y., Lewis, A. S., Gallagher, J. J., Wadman, W. J., Baram, T. Z., and Chetkovich, D. M. (2011) Trafficking and gating of hyperpolarization-activated cyclic nucleotide-gated channels are regulated by interaction with tetratricopeptide repeat-containing Rab8b-interacting protein (TRIP8b) and cyclic AMP at distinct sites. *J. Biol. Chem.* **286,** 20823–20834
21. Bankston, J. R., Camp, S. S., DiMaio, F., Lewis, A. S., Chetkovich, D. M., and Zagotta, W. N. (2012) Structure and stoichiometry of an accessory subunit TRIP8b interaction with hyperpolarization-activated cyclic nucleotide-gated channels. *Proc. Natl. Acad. Sci. U.S.A.* **109,** 7899–7904
22. Gravante, B., Barbuti, A., Milanesi, R., Zappi, I., Viscomi, C., and DiFrancesco, D. (2004) Interaction of the pacemaker channel HCN1 with filamin A. *J. Biol. Chem.* **279,** 43847–43853
23. Barbuti, A., Terragni, B., Brioschi, C., and DiFrancesco, D. (2007) Localization of f-channels to caveolae mediates specific β2-adrenergic receptor modulation of rate in sinoatrial myocytes. *J. Mol. Cell Cardiol.* **42,** 71–78
24. Michels, G., Er, F., Khan, I. F., Endres-Becker, J., Brandt, M. C., Gassanov, N., Johns, D. C., and Hoppe, U. C. (2008) K^+ channel regulator KCR1 suppresses heart rhythm by modulating the pacemaker current If. *PLoS One* **3,** e1511
25. Decher, N., Bundis, F., Vajna, R., and Steinmeyer, K. (2003) KCNE2 modulates current amplitudes and activation kinetics of HCN4: influence of KCNE family members on HCN4 currents. *Pflugers Arch.* **446,** 633–640
26. Kimura, K., Kitano, J., Nakajima, Y., and Nakanishi, S. (2004) Hyperpolarization-activated, cyclic nucleotide-gated HCN2 cation channel forms a protein assembly with multiple neuronal scaffold proteins in distinct modes of protein-protein interaction. *Genes Cells* **9,** 631–640
27. Hammelmann, V., Zong, X., Hofmann, F., Michalakis, S., and Biel, M. (2011) The cGMP-dependent protein kinase II Is an inhibitory modulator of the hyperpolarization-activated HCN2 channel. *PLoS One* **6,** e17078
28. Poolos, N. P., Bullis, J. B., and Roth, M. K. (2006) Modulation of h-channels in hippocampal pyramidal neurons by p38 mitogen-activated protein kinase. *J. Neurosci.* **26,** 7995–8003
29. Li, C. H., Zhang, Q., Teng, B., Mustafa, S. J., Huang, J. Y., and Yu, H. G. (2008) Src tyrosine kinase alters gating of hyperpolarization-activated HCN4 pacemaker channel through Tyr531. *Am. J. Physiol. Cell Physiol.* **294,** C355–C362
30. Zong, X., Eckert, C., Yuan, H., Wahl-Schott, C., Abicht, H., Fang, L., Li, R., Mistrik, P., Gerstner, A., Much, B., Baumann, L., Michalakis, S., Zeng, R., Chen, Z., and Biel, M. (2005) A novel mechanism of modulation of hyperpolarization-activated cyclic nucleotide-gated channels by Src kinase. *J. Biol. Chem.* **280,** 34224–34232
31. Moosmang, S., Biel, M., Hofmann, F., and Ludwig, A. (1999) Differential distribution of four hyperpolarization-activated cation channels in mouse brain. *Biol. Chem.* **380,** 975–980
32. Notomi, T., and Shigemoto, R. (2004) Immunohistochemical localization of Ih channel subunits, HCN1–4, in the rat brain. *J. Comp Neurol.* **471,** 241–276
33. Fenske, S., Mader, R., Scharr, A., Paparizos, C., Cao-Ehlker, X., Michalakis, S., Shaltiel, L., Weidinger, M., Stieber, J., Feil, S., Feil, R., Hofmann, F., Wahl-Schott, C., and Biel, M. (2011) HCN3 Contributes to the Ventricular Action Potential Waveform in the Murine Heart. *Circ. Res.* **109,** 1015–1023
34. Mistrík, P., Mader, R., Michalakis, S., Weidinger, M., Pfeifer, A., and Biel, M. (2005) The murine HCN3 gene encodes a hyperpolarization-activated cation channel with slow kinetics and unique response to cyclic nucleotides. *J. Biol. Chem.* **280,** 27056–27061
35. Chaplan, S. R., Guo, H. Q., Lee, D. H., Luo, L., Liu, C., Kuei, C., Velumian, A. A., Butler, M. P., Brown, S. M., and Dubin, A. E. (2003) Neuronal hyperpolarization-activated pacemaker channels drive neuropathic pain. *J. Neurosci.* **23,** 1169–1178
36. Hurtado, R., Bub, G., and Herzlinger, D. (2010) The pelvis-kidney junction contains HCN3, a hyperpolarization-activated cation channel that triggers ureter peristalsis. *Kidney Int.* **77,** 500–508
37. Stogios, P. J., Downs, G. S., Jauhal, J. J., Nandra, S. K., and Privé, G. G. (2005) Sequence and structural analysis of BTB domain proteins. *Genome Biol.* **6,** R82
38. Borinstein, S. C., Hyatt, M. A., Sykes, V. W., Straub, R. E., Lipkowitz, S., Boulter, J., and Bogler, O. (2000) SETA is a multifunctional adapter protein with three SH3 domains that binds Grb2, Cbl, and the novel SB1 proteins. *Cell Signal.* **12,** 769–779
39. Perrière, G., and Gouy, M. (1996) WWW-query: an on-line retrieval system for biological sequence banks. *Biochimie* **78,** 364–369
40. Zong, X., Krause, S., Chen, C. C., Krüger, J., Gruner, C., Cao-Ehlker, X., Fenske, S., Wahl-Schott, C., and Biel, M. (2012) Regulation of Hyperpolarization-activated Cyclic Nucleotide-gated (HCN) Channel Activity by cCMP. *J. Biol. Chem.* **287,** 26506–26512
41. Moosmang, S., Stieber, J., Zong, X., Biel, M., Hofmann, F., and Ludwig, A. (2001) Cellular expression and functional characterization of four hyper-

polarization-activated pacemaker channels in cardiac and neuronal tissues. *Eur. J. Biochem.* **268,** 1646–1652
42. Zong, X., Schieder, M., Cuny, H., Fenske, S., Gruner, C., Rötzer, K., Griesbeck, O., Harz, H., Biel, M., and Wahl-Schott, C. (2009) The two-pore channel TPCN2 mediates NAADP-dependent Ca(2+)-release from lysosomal stores. *Pflugers Arch* **458,** 891–899
43. Ludwig, A., Budde, T., Stieber, J., Moosmang, S., Wahl, C., Holthoff, K., Langebartels, A., Wotjak, C., Munsch, T., Zong, X., Feil, S., Feil, R., Lancel, M., Chien, K. R., Konnerth, A., Pape, H. C., Biel, M., and Hofmann, F. (2003) Absence epilepsy and sinus dysrhythmia in mice lacking the pacemaker channel HCN2. *EMBO J.* **22,** 216–224
44. Michalakis, S., Zong, X., Becirovic, E., Hammelmann, V., Wein, T., Wanner, K. T., and Biel, M. (2011) The glutamic acid-rich protein is a gating inhibitor of cyclic nucleotide-gated channels. *J. Neurosci.* **31,** 133–141
45. Scanlan, M. J., Gordan, J. D., Williamson, B., Stockert, E., Bander, N. H., Jongeneel, V., Gure, A. O., Jäger, D., Jäger, E., Knuth, A., Chen, Y. T., and Old, L. J. (1999) Antigens recognized by autologous antibody in patients with renal-cell carcinoma. *Int. J. Cancer* **83,** 456–464
46. Gulbis, J. M., Zhou, M., Mann, S., and MacKinnon, R. (2000) Structure of the cytoplasmic beta subunit-T1 assembly of voltage-dependent K+ channels. *Science* **289,** 123–127
47. Smith, T. F. (2008) Diversity of WD-repeat proteins. *Sub-cellular Biochem.* **48,** 20–30
48. Smith, T. F., Gaitatzes, C., Saxena, K., and Neer, E. J. (1999) The WD repeat: a common architecture for diverse functions. *Trends Biochem. Sci.* **24,** 181–185
49. Yan, R. T., Ma, W. X., and Wang, S. Z. (2001) neurogenin2 elicits the genesis of retinal neurons from cultures of nonneural cells. *Proc. Natl. Acad. Sci. U.S.A.* **98,** 15014–15019
50. Melnick, A., Ahmad, K. F., Arai, S., Polinger, A., Ball, H., Borden, K. L., Carlile, G. W., Prive, G. G., and Licht, J. D. (2000) In-depth mutational analysis of the promyelocytic leukemia zinc finger BTB/POZ domain reveals motifs and residues required for biological and transcriptional functions. *Mol. Cell. Biol.* **20,** 6550–6567
51. Kang, M. I., Kobayashi, A., Wakabayashi, N., Kim, S. G., and Yamamoto, M. (2004) Scaffolding of Keap1 to the actin cytoskeleton controls the function of Nrf2 as key regulator of cytoprotective phase 2 genes. *Proc. Natl. Acad. Sci. U.S.A.* **101,** 2046–2051
52. Pintard, L., Willis, J. H., Willems, A., Johnson, J. L., Srayko, M., Kurz, T., Glaser, S., Mains, P. E., Tyers, M., Bowerman, B., and Peter, M. (2003) The BTB protein MEL-26 is a substrate-specific adaptor of the CUL-3 ubiquitin-ligase. *Nature* **425,** 311–316
53. Correale, S., Pirone, L., Di Marcotullio, L., De Smaele, E., Greco, A., Mazzà, D., Moretti, M., Alterio, V., Vitagliano, L., Di Gaetano, S., Gulino, A., and Pedone, E. M. (2011) Molecular organization of the cullin E3 ligase adaptor KCTD11. *Biochimie* **93,** 715–724
54. Schwenk, J., Metz, M., Zolles, G., Turecek, R., Fritzius, T., Bildl, W., Tarusawa, E., Kulik, A., Unger, A., Ivankova, K., Seddik, R., Tiao, J. Y., Rajalu, M., Trojanova, J., Rohde, V., Gassmann, M., Schulte, U., Fakler, B., and Bettler, B. (2010) Native GABA(B) receptors are heteromultimers with a family of auxiliary subunits. *Nature* **465,** 231–235
55. Dementieva, I. S., Tereshko, V., McCrossan, Z. A., Solomaha, E., Araki, D., Xu, C., Grigorieff, N., and Goldstein, S. A. (2009) Pentameric assembly of potassium channel tetramerization domain-containing protein 5. *J. Mol. Biol.* **387,** 175–191
56. Metz, M., Gassmann, M., Fakler, B., Schaeren-Wiemers, N., and Bettler, B. (2011) Distribution of the auxiliary GABAB receptor subunits KCTD8, 12, 12b, and 16 in the mouse brain. *J Comp Neurol* **519,** 1435–1454